Available online at www.sciencedirect.com
SCIENCE DIRECT®
International Journal of Heat and Mass Transfer 49 (2006) 4360–4371
International Journal of HEAT and MASS TRANSFER
www.elsevier.com/locate/ijhmt

An investigation of heat transfer of a reciprocating piston

Wu-Shung Fu *, Sin-Hong Lian, Liao-Ying Hao

Department of Mechanical Engineering, National Chiao Tung University, 1001 Ta Hsueh Road, Hsinchu 30056, Taiwan, ROC

Received 17 November 2005; received in revised form 22 April 2006
Available online 17 July 2006

Abstract

A numerical simulation of a reciprocating piston cooled by fluid is performed to investigate effects of frequency, amplitude and Reynolds number on heat transfer rate of the piston. For facilitating the analyses, the model of the reciprocating piston is replaced by a "∏" shape cooling channel. This subject belongs to a kind of moving boundary problems, and the Finite Element Method and arbitrary Lagragian–Eulerian Kinematics description method are then utilized. The heat transfer mechanisms affected by the main parameters of frequency, amplitude and Reynolds number are discussed in detail. The results show that the heat transfer mechanisms influenced by the frequency are more remarkable than those influenced by the amplitude and Reynolds number. Besides, the larger the above three parameters are, the apparent enhancements of heat transfer are usually obtained.

Keywords: Moving boundary problems; Piston cooling; Forced convection

1. Introduction

Protecting the piston free from heat damage could effectively enhance the thermal efficiency of the heat engine [1]. Lots of studies were then to investigate similar object recently.

For the complex geometry and reciprocating motion of the piston in the simulation of cooling system, it is usually substituted by a straight channel being subject to up and down reciprocating motion or pulsating cooling fluids flowing through a straight channel. Grassma and Tuma's results [2] indicated that the mass transfer could achieve a level of about 2.5 times of the stationary case. Patera and Mikic [3] showed that the above enhancement might result from flows mixing due to hydrodynamic instability induced by pulsating flows. The results of Kim et al. [4] were that the pulsating amplitude affected heat transfer significantly and a heat transfer impediment relative to the non-pulsating situation might occur in the thermally developing flow region. Nishimura [5–8] utilized a sinusoidal wavy-walled channel replacing a smooth duct to investigate heat transfer enhancement by pulsating and oscillatory flows numerically and experimentally, and the results indicated that the higher heat transfer rates relative to the small duct were achieved, and the flow patterns which affected heat transfer rate directly were influenced by the frequency of oscillatory remarkably. Chiu and Kuo [9] investigated turbulent heat transfer and predicted wall heat flux in reciprocating engine by using an algebraic grid generation technique. The results showed that increasing the curvature of the cylinder head will increase the strength of induced squish flow and wall heat flux. Cheng and Su [10] conducted an experimental work to investigate influence of reciprocating motion on heat transfer inside a ribbed enclosure and showed that at the highest reciprocating speed, the heat transfer was enhanced about 145% of the equivalent stationary case. Chang and Su [1] modified the experiment and gained the results which at a pulsating number of 10.5, the time-average Nusselt number could reach about 165% of the stationary one. Cheng and Hung [11] developed a solution method for predicting unsteady flow and thermal fields in a reciprocating piston-cylinder assembly. The results showed that

* Corresponding author. Tel.: +886 3 5712121x55110; fax: +886 3 5720634.
E-mail address: wsfu@cc.nctu.edu.tw (W.-S. Fu).

0017-9310/$ - see front matter © 2006 Elsevier Ltd. All rights reserved.
doi:10.1016/j.ijheatmasstransfer.2006.04.036

Nomenclature

f_c	reciprocating frequency of the piston (s^{-1})
F_c	dimensionless reciprocating frequency of the piston
h_0	dimensional height of the piston (m)
h_1	dimensional height of the inlet channel and outlet channel (m)
l_c	reciprocating amplitude of the piston (m)
L_c	dimensionless reciprocating amplitude of the piston
$\dot{M}$	dimensionless mass flow rate
Nu_X	local Nusselt number
$\overline{Nu}_X$	average Nusselt number on the heat surface
$\overline{Nu}$	time-average Nusselt number per cycle
p	dimensional pressure ($N\,m^{-2}$)
p_∞	reference pressure ($N\,m^{-2}$)
P	dimensionless pressure
Pr	Prandtl number
Re	Reynolds number
t	dimensional time (s)
T	dimensional temperature (K)
T_0	dimensional temperature of the inlet fluid (K)
T_h	dimensional temperature of the heat surface (K)
u, v	dimensional velocities of in x- and y-directions ($m\,s^{-1}$)
U, V	dimensionless velocities of in X- and Y-directions
v_0	dimensional velocities of the inlet fluid ($m\,s^{-1}$)
V_0	dimensionless velocities of the inlet fluid
v_c	dimensional reciprocating velocity of the piston ($m\,s^{-1}$)
V_c	dimensionless reciprocating velocity of the piston
v_m	dimensional maximum reciprocating velocity of the piston ($m\,s^{-1}$)
V_m	dimensionless maximum reciprocating velocity of the piston
$\hat{v}$	dimensional mesh velocity in y-direction ($m\,s^{-1}$)
$\hat{V}$	dimensionless mesh velocity in y-direction
w_0	dimensional width of the piston (m)
w	dimensional width of the channel (m)
W	dimensionless width of the channel
x, y	dimensional Cartesian coordinates (m)
X, Y	dimensionless Cartesian coordinates

Greek symbols

α	thermal diffusivity ($m^2\,s^{-1}$)
Φ	computational variables
λ	penalty parameter
ν	kinematics viscosity ($m^2\,s^{-1}$)
η_0	total length of the moving mesh region
η_1	length counted from the bottom of the moving mesh region
θ	dimensionless temperature
ρ	density ($kg\,m^{-3}$)
τ	dimensionless time
τ_p	dimensionless time of one oscillating cycle
Ψ	dimensionless stream function

Other

$\|$	absolute value

the two-stage pressure correction procedure could be readily incorporated into existing numerical techniques to yield reasonably accurate results. Sert and Beskok [12] studied oscillatory flow forced convection in microheat spreaders numerically. The results showed that a fluid with low viscosity, low density, and high thermal conductivity is desired in coolant selection. Khaled and Vafai [13] considered the influence of fluids inertia and the effects of the presence of a magnetic field normal to the direction of the flow of an electrically conducting fluid on flow and heat transfer inside a non-isothermal and incompressible thin film undergoing oscillatory squeezing. It was found the flow instabilities increase as the squeezing Reynolds number increases and they decrease as the Hartmann number increases, and Nusselt number would be affected by the increased squeezing Reynolds number. Afterward, Chang et al. [14] set an anti-gravity open thermosiphon system which was a more realistic model of a cooling system of piston than the ones proposed before to study the heat transfer of piston under the conditions of cooling fluids flowing through. Effects of inertia, pulsating and buoyancy forces were taken into consideration and a correlation formula which was consistent with the heat transfer physics expressed with dimensionless temperature was proposed.

The model of the cooling fluid flow being parallel to the heat surface was adopted in the stated literature. However, the cooling fluid flow in the cooling system for the realistic situation of piston was vertical to the reciprocating heat surface. The later phenomenon belongs to a kind of moving boundary problem and is seldom investigated relatively.

Therefore, the aim of the study is to utilize Arbitrary Lagrangian–Eulerian method (ALE method) which is appropriate for moving boundary problems and to investigate the heat transfer rate of cooling fluid to flow into a piston vertically. For satisfying the demand of numerical computation, the cooling system is assumed as a "$\sqcap$" shape channel. The top side of horizontal channel of the "$\sqcap$" shape channel is regarded as the bottom surface of the piston which reciprocates and maintains at a high temperature. The cooling fluid flows in and out from the left and right channels, respectively. In connection with the horizontal channel and the left and right channels, baffle channels which could elongate and shorten accompanying

with the reciprocating motion of piston are installed. Important parameters of mass flow rate of cooling fluid, frequency and amplitude of reciprocating motion are considered, and the effects of the above parameters on the heat transfer rate of the piston are examined in detail.

2. Physical model

A physical model of two-dimensional "∏" shape cooling channel simulating a piston used in this study is shown in Fig. 1. The total width and length of the cooling channel are w_0 and h_0, respectively, and the width of the cooling channel is w. The top surface $\overline{BC}$ is heat surface and at constant temperature T_H which is cooled down by the inlet cooling fluid of which the temperature and velocity are T_0 and v_0, respectively. The other surfaces of the cooling channel are insulated. The region between $\overline{OP}$ and $\overline{MN}$ is flexible of which the length is w and could be elongated to $2w$. The adjustable length w is utilized to simulate the moving distance of the reciprocating motion of the piston. Therefore, the computation grid sizes in this region are extensible. As the channel moves upward, the $\overline{MN}$ is fixed and $\overline{OP}$ moves upward with velocity v_c which causes the stated region to elongate, and the maximum moving distance is w. Afterward, the $\overline{OP}$ moves downward and returns to the original position. The moving velocity of the horizontal channel is naturally the same with the moving velocity of the $\overline{OP}$. For satisfying convergence conditions of computation, the right channel length h_1 is long enough and the exit conditions of temperature and velocity are both fully developed. The reciprocating velocity of the horizontal channel is v_c, and can be expressed in terms of $v_c = v_m \sin(2\pi f_c t)$, where v_m is the maximum reciprocating velocity of the piston and equals to $2\pi l_c f_c$. When the channel moves reciprocally which affects the behaviors of the cooling fluid transiently, the motions of the cooling fluid become time-dependent which could be classified into a kind of moving boundary problems. As a result, the ALE method is properly employed to analyze this study.

For facilitating the analysis, the following assumptions are made:

(1) The fluid is air and the flow field is two-dimensional, incompressible and laminar.
(2) The fluid properties are constant and the effect of the gravity is neglected.

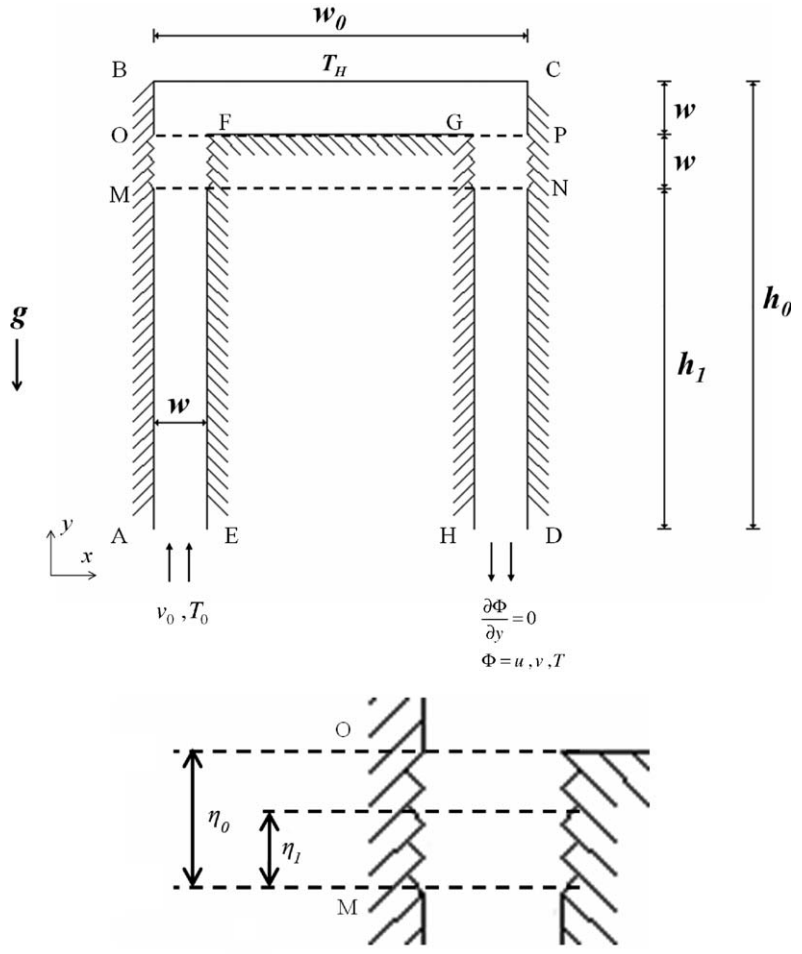

Fig. 1. Physical model.

(3) The no-slip condition is held on all boundaries. Thus, the fluid velocities on moving boundaries are equal to the boundary moving velocities.

Based upon the characteristics scales of w, v_0, ρv_0^2, and T_0, the dimensionless variables are defined as follows:

$$X=\frac{x}{w},\quad Y=\frac{y}{w},\quad U=\frac{u}{v_0},\quad V=\frac{v}{v_0},\quad \widehat{V}=\frac{\hat{v}}{v_0}$$
$$V_{\mathrm{m}}=\frac{v_{\mathrm{m}}}{v_0},\quad V_{\mathrm{c}}=\frac{v_{\mathrm{c}}}{v_0},\quad F_{\mathrm{c}}=\frac{f_{\mathrm{c}}w}{v_0},\quad P=\frac{p-p_\infty}{\rho v_0^2} \tag{1}$$
$$\tau=\frac{tv_0}{w},\quad \theta=\frac{T-T_0}{T_{\mathrm{h}}-T_0},\quad Re=\frac{v_0 w}{\nu},\quad Pr=\frac{\nu}{\alpha}$$

where $\hat{v}$ is defined as the mesh velocity, f_{c}, v_{m}, v_{c} are the reciprocating frequency, the maximum reciprocating velocity, and the instant reciprocating velocity of the piston, respectively.

According to the above assumptions and dimensionless variables, the dimensionless ALE governing equations are expressed as the following equations:

Continuity equation

$$\frac{\partial U}{\partial X}+\frac{\partial V}{\partial Y}=0 \tag{2}$$

Momentum equation

$$\frac{\partial U}{\partial \tau}+U\frac{\partial U}{\partial X}+(V-\widehat{V})\frac{\partial U}{\partial Y}=-\frac{\partial P}{\partial X}+\frac{1}{Re}\left(\frac{\partial^2 U}{\partial X^2}+\frac{\partial^2 U}{\partial Y^2}\right) \tag{3}$$

$$\frac{\partial V}{\partial \tau}+U\frac{\partial V}{\partial X}+(V-\widehat{V})\frac{\partial V}{\partial Y}=-\frac{\partial P}{\partial Y}+\frac{1}{Re}\left(\frac{\partial^2 V}{\partial X^2}+\frac{\partial^2 V}{\partial Y^2}\right) \tag{4}$$

Energy equation

$$\frac{\partial \theta}{\partial \tau}+U\frac{\partial \theta}{\partial X}+(V-\widehat{V})\frac{\partial \theta}{\partial Y}=\frac{1}{RePr}\left(\frac{\partial^2 \theta}{\partial X^2}+\frac{\partial^2 \theta}{\partial Y^2}\right) \tag{5}$$

In this study, the cooling channel moves upward and downward in vertical direction only, therefore, the horizontal mesh velocity is absent in the above governing equations. According to ALE method, the mesh velocity $\widehat{V}$ is linearly distributed in the region between $\overline{MN}$ (fixed) and $\overline{OP}$ (movable). In the other regions, the mesh velocities $\widehat{V}$ are all set to 0.

Steady states of flow and thermal fields are used as initial conditions before the piston reciprocating. Furthermore, the boundary conditions are as follows:

Inlet $\overline{AE}$

$$U=0,\quad V=1,\quad \theta=0 \tag{6}$$

Outlet $\overline{HD}$

$$\frac{\partial U}{\partial Y}=0,\quad \frac{\partial V}{\partial Y}=0,\quad \frac{\partial \theta}{\partial Y}=0 \tag{7}$$

Flexible walls between $\overline{OP}$ and $\overline{MN}$

$$U=0,\quad V=\begin{cases}0 & \tau=0\\ V_{\eta_1} & \tau>0\end{cases},\quad \frac{\partial \theta}{\partial X}=0 \tag{8}$$

where V_{η_1} is the mesh velocity of the position η_1 and proportional to the distance between $\overline{MN}$ and $\overline{OP}$, and is defined as following equation:

$$V_{\eta_1}=\frac{\eta_1}{\eta_0}\cdot V_{\mathrm{c}} \tag{9}$$

Walls of $\overline{OB}$ and $\overline{PC}$

$$U=0,\quad V=\begin{cases}0 & \tau=0\\ V_{\mathrm{c}} & \tau>0\end{cases},\quad \frac{\partial \theta}{\partial X}=0 \tag{10}$$

Wall $\overline{FG}$

$$U=0,\quad V=\begin{cases}0 & \tau=0\\ V_{\mathrm{c}} & \tau>0\end{cases},\quad \frac{\partial \theta}{\partial Y}=0 \tag{11}$$

Wall $\overline{BC}$

$$U=0,\quad V=\begin{cases}0 & \tau=0\\ V_{\mathrm{c}} & \tau>0\end{cases},\quad \theta=1 \tag{12}$$

Other walls

$$U=0,\quad V=0,\quad \frac{\partial \theta}{\partial X}=0 \tag{13}$$

3. Numerical method

The governing equations and boundary conditions are solved through the Galerkin finite element formulation and a backward scheme is adopted to deal with the time terms of the governing equations. The pressure is eliminated from the governing equations using the consistent penalty method [15]. The velocity and temperature terms are expressed as quadrilateral element and eight-node quadratic Lagrangian interpolation utilized to simplify the non-linear terms in the momentum equations. The discretion processes of the governing equations are similar to the one used in Fu et al. [16]. Then, the momentum equations (3) and (4) can be expressed as the following matrix form:

$$\sum_1^{n_e}\left([A]^{(e)}+[K]^{(e)}+\lambda[L]^{(e)}\right)\{q\}^{(e)}_{\tau+\Delta\tau}=\sum_1^{n_e}\{f\}^{(e)} \tag{14}$$

where

$$\left(\{q\}^{(e)}_{\tau+\Delta\tau}\right)^{\mathrm{T}}=\langle U_1,U_2,\ldots,U_8,V_1,V_2,\ldots,V_8\rangle^{m+1}_{\tau+\Delta\tau} \tag{15}$$

$[A]^{(e)}$ includes the (m)th iteration values of U and V at time $\tau+\Delta\tau$; $[K]^{(e)}$ includes the shape function, $\widehat{V}$, and time differential terms; $[L]^{(e)}$ includes the penalty function; $[f]^{(e)}$ includes the known values of U and V at time τ and (m)th iteration values of U and V at time $\tau+\Delta\tau$.

The energy equation (5) can be expressed as the following matrix form:

$$\sum_1^{n_e}\left([M]^{(e)}+[Z]^{(e)}\right)\{c\}^{(e)}_{\tau+\Delta\tau}=\sum_1^{n_e}\{r\}^{(e)} \tag{16}$$

where

$$\left(\{c\}^{(e)}_{\tau+\Delta\tau}\right)^{\mathrm{T}} = \langle\theta_1, \theta_2, \ldots, \theta_8\rangle^{m+1}_{\tau+\Delta\tau} \tag{17}$$

$[M]^{(e)}$ includes the values of U and V at time $\tau+\Delta\tau$; $[Z]^{(e)}$ includes the shape function, $\widehat{V}$, and time differential terms; $[r]^{(e)}$ includes the known values of θ at time τ.

In Eqs. (14) and (16), Gaussian quadrature procedure are conveniently used to execute the numerical integration. The terms with the penalty parameter λ are integrated by 2×2 Gaussian quadrature, and the other terms are integrated by 3×3 Gaussian quadrature. The value of penalty parameter λ used in this study is 10^6. The frontal method solver is applied to solve Eqs. (14) and (16).

A brief outline of the solution procedures are described as follows:

(1) Determine the optimal mesh distribution and number of the elements and nodes.
(2) Solve the values of the U, V, and θ at the steady state and regard them as the initial values.
(3) Determine the time step $\Delta\tau$ and the mesh velocity $\widehat{V}$ of the computational meshes.
(4) Update the coordinates of the nodes and examine the determinant of the Jacobian transformation matrix to ensure the one to one mapping to be satisfied during the Gaussian quadrature numerical integration.
(5) Solve Eq. (14), until the following criteria for convergence are satisfied:

$$\left|\frac{\Phi^{m+1}-\Phi^{m}}{\Phi^{m+1}}\right|_{\tau+\Delta\tau} < 10^{-3} \tag{18}$$

where $\Phi = U$ and V, and substitute the U and V into Eq. (16) to obtain θ.
(6) Continue the next time step calculation until periodic solutions are attained.

4. Results and discussion

The working fluid is air with $Pr = 0.71$. The main parameters of Reynolds number Re, maximum oscillating velocity V_{m}, oscillating frequency F_{c}, and oscillating amplitude L_{c} are examined and the combinations of these parameters are tabulated in Table 1.

The local Nusselt number Nu_X at time τ and average Nusselt number $\overline{Nu}_X$ on the high temperature surface at time τ are calculated by the following equations, respectively:

$$Nu_X = -\frac{\partial\theta}{\partial Y} \tag{19}$$

$$\overline{Nu}_X = \frac{1}{w}\int_{\overline{BC}} Nu_X \,\mathrm{d}X \tag{20}$$

Table 1
Computed parameter combinations

	Re	V_{m}	F_{c}	L_{c}	$\overline{Nu}$	$\frac{\overline{Nu}_{\mathrm{Case}\,n}}{\overline{Nu}_{\mathrm{Stationary}}}$
Stationary	200	–	–	–	1.783	1.000
Case 1	200	0.157	0.1	0.25	3.579	2.007
Case 2	200	0.314	0.2	0.25	3.958	2.220
Case 3	200	0.628	0.4	0.25	4.060	2.277
Case 4	200	0.314	0.1	0.5	3.646	2.045
Case 5	200	0.628	0.1	1	3.904	2.190
Case 6	500	0.157	0.1	0.25	5.727	3.212
Case 7	750	0.157	0.1	0.25	7.202	4.039

The time-average Nusselt number per cycle $\overline{Nu}$ is defined as

$$\overline{Nu} = -\frac{1}{\tau_p}\int_0^{\tau_p} \overline{Nu}_X \,\mathrm{d}\tau, \tag{21}$$

in which τ_p is a cycle time.

For matching the boundary conditions at the outlet of the channel, the length from the horizontal channel to the outlet of the right channel is determined by numerical tests and about to 50. To obtain an optimal computational mesh, three different non-uniform distributed elements, which provide a finer element resolution in the horizontal channel and vertical channel neighboring the horizontal channel, are used for the mesh tests. Fig. 2 shows the velocity and temperature profiles along the horizontal and vertical lines through the center of the horizontal channel and parallel the X-axis and Y-axis, respectively, at a steady state under $Re = 750$. Based upon the results, the computational mesh with 8025 elements, which is corresponding to 25,176 nodes, is used for all cases in this study. In additional, an implicit scheme is employed to deal with the time differential term of the governing equations. The time step $\Delta\tau = \frac{1}{48F_{\mathrm{c}}}$ is chosen for all cases, i.e. totally 48 time steps are required to achieve one periodic cycle.

The dimensionless stream function Ψ is defined as

$$U = \frac{\partial\Psi}{\partial Y}, \quad V = -\frac{\partial\Psi}{\partial X} \tag{22}$$

For clearly indicating the variations of the flow and thermal fields, the streamlines and isothermal lines in the vicinity of the horizontal channel are presented only. Besides, the sign "↑" in the subsequent figures is to indicate the moving direction of the horizontal channel.

Fig. 3 shows the variations of the streamlines and isothermal lines for case 2 during one periodical cycle. The streamlines and isothermal lines at the time $\tau = 4\tau_p/4$ (Fig. 3(a1) and (b1)) are identical with those at the time $\tau = 4\tau_p/4$ (Fig. 3(a5) and (b5)), which means that the variations of the flow and thermal fields become a periodical motion with time. The main direction of cooling fluid in the horizontal channel is to the right and vertical to the direction of the cooling fluid flow from the left channel. The impingement region caused by the cooling fluid on the top surface of the horizontal channel then slightly leans to the right side ($x \fallingdotseq$ 1–2) relative to the original flowing direction of the left

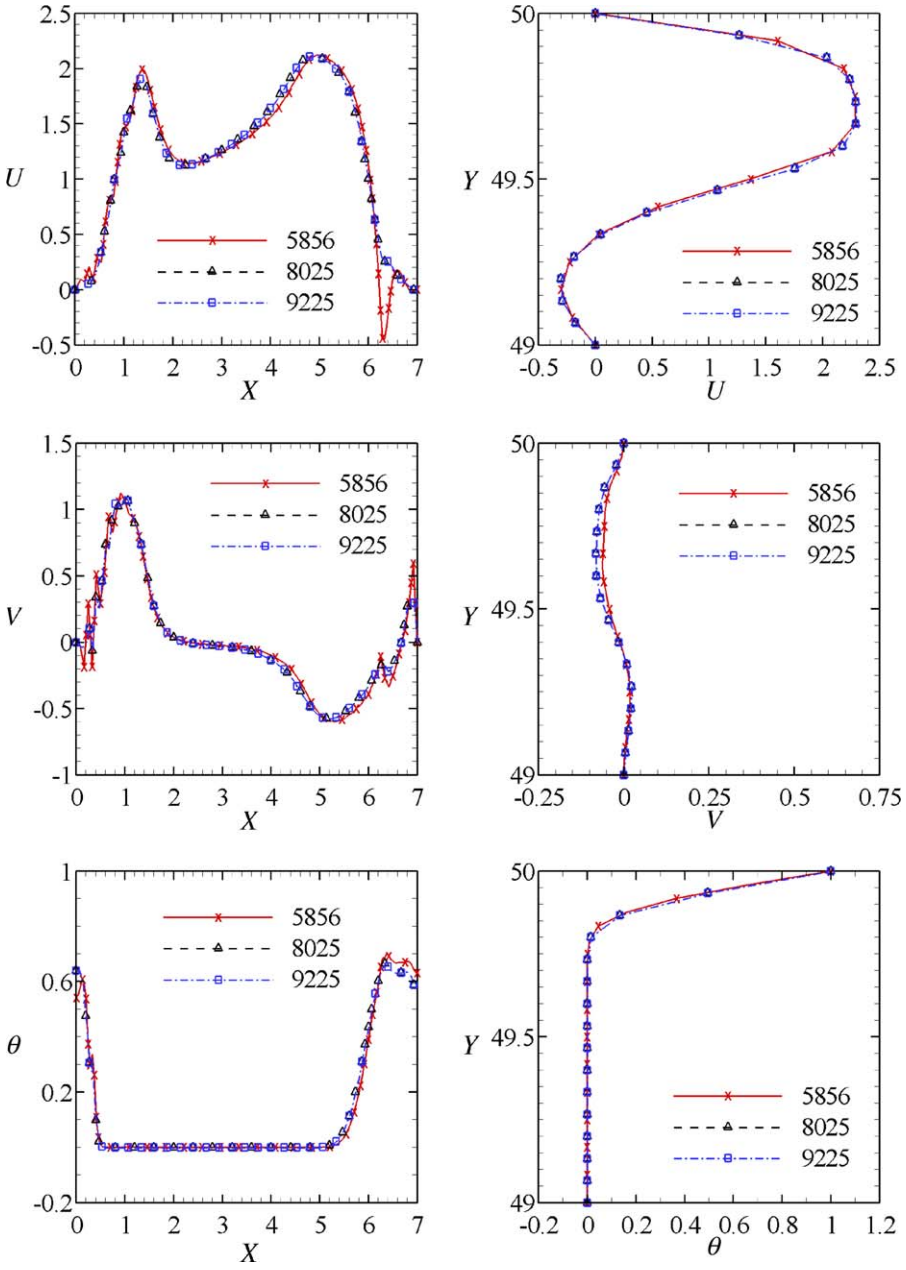

Fig. 2. Comparison of the velocity and temperature profiles along the horizontal and vertical lines through the center of the horizontal channel and parallel the X-axis and Y-axis, respectively, for different meshes.

channel. The cooling fluid turns the flowing direction vertically in the horizontal channel which causes two circulation zones formed on the left top and left bottom surfaces of the horizontal channel, respectively. Due to the rebound of the stated impingement of cooling fluid, a small circulation region near the center region of the top surface is observed. As the cooling fluid flows out from the exit of the horizontal channel, the similar phenomena which occur in the inlet region mentioned above are found out near the exit region of the horizontal channel.

In Fig. 3(a2), the upward velocity of the channel is accelerated to the maximum magnitude. The no-slip condition is hold on the walls of the horizontal channel which results in the flow direction of the cooling fluid in the horizontal channel being from the bottom to top surfaces, and inclining from the bottom left to the upper right due to the flow direction of the cooling fluid in the horizontal channel. However, the flow direction of cooling fluid in the right channel is downward which is opposite to the moving direction of the channel. Mutual influence between the motions of the channel and cooling fluid, the flow directions of cooling fluid are then distorted in the right channel.

In Fig. 3(a3), the moving velocity of the channel is decelerated to 0 which means the upward effect to disappear. The streamlines distribution is then changed and distorted which is similar to those indicated in Fig. 3(a1).

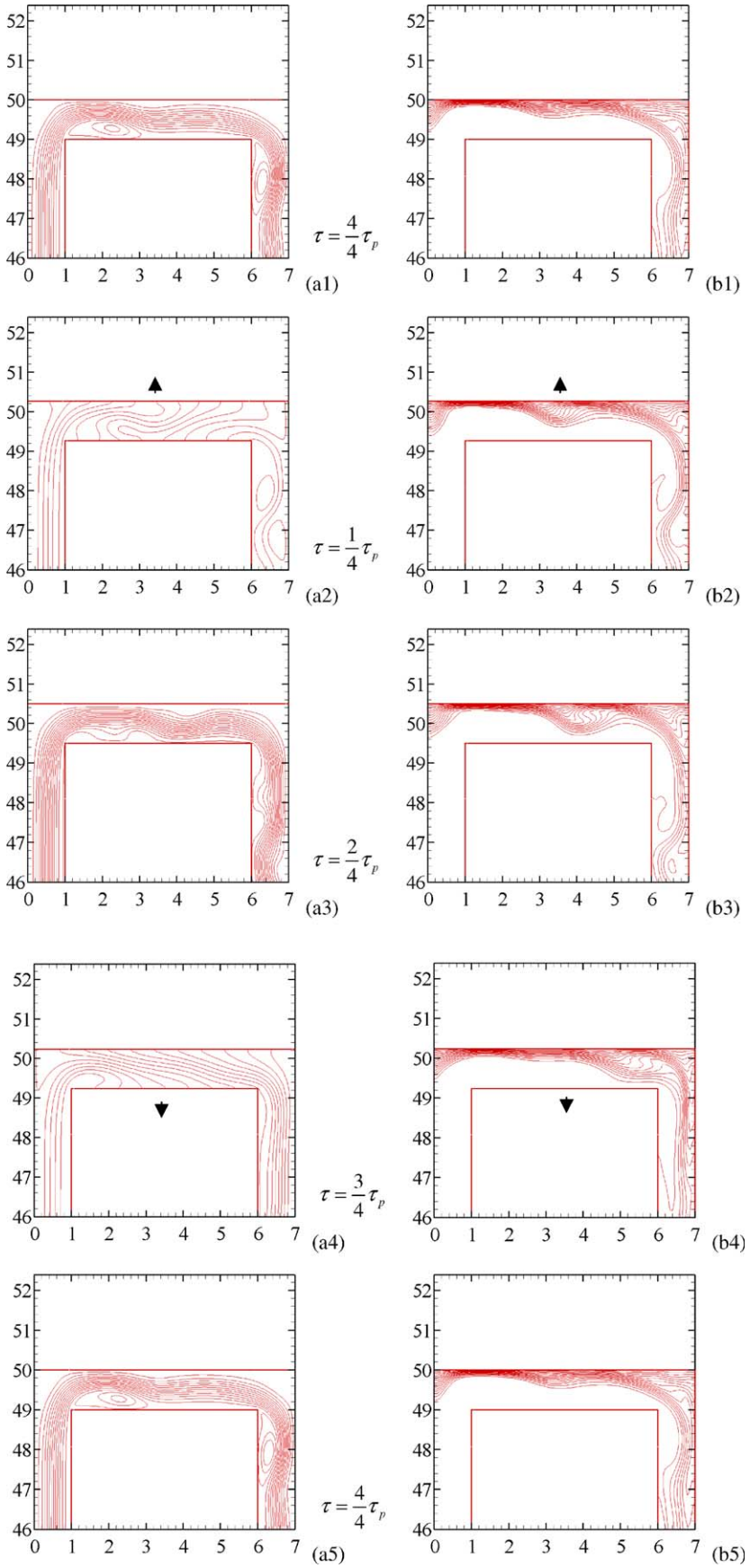

Fig. 3. The variations of the streamlines and isothermal lines during one periodic cycle for case 2.

Shown in Fig. 3(a4), the downward velocity of the channel is accelerated to the maximum magnitude. The moving directions between the channel and cooling fluid are opposite in the left channel and same in the right channel, respectively, which cause the variations of streamline distributions in both the channels to be different from those indicated in Fig. 3(a2). In the horizontal channel, the flow directions of the cooling fluid are from the top to bottom surfaces, and incline from the upper left to the bottom right caused by the flow direction of the cooling fluid in the horizontal channel. In Fig. 3(a5), the phenomena are at the end of a periodical cycle, then the variations of the streamline distributions are consistent with those shown in Fig. 3(a1).

As for the variations of the isothermal lines, since the thermal boundary layer still attaches to the top surface of the horizontal channel tightly in spite of the reciprocating motion of the channel. As a result, the variations of isothermal lines are more monotonous than those of streamlines. Shown in Fig. 3(b1), according to the distributions of streamlines, the distributions of isothermal lines are dense in the stated impingement region, and are dispersed in the circulation region mentioned in Fig. 3(a1) and the left and right corners. Around the circulation region, the distribution of the isothermal lines becomes a convex region. Accompanying with the flowing of the cooling fluid, the above convex region gradually moves to the right (Fig. 3(b2)), and grows up (Fig. 3(b3)) and almost touches the bottom surface of the horizontal channel (Fig. 3(b4)), in the meanwhile, a nebulous small convex region could be observed behind the stated convex region and prepares to grow up. Finally, the convex region flows into the right channel. The behaviors of the convex region are somewhat similar to the wavy flow.

Fig. 4 indicates the distributions of the local Nusselt number Nu_X on the heat surface at the $\tau_p/4$, $2\tau_p/4$, $3\tau_p/4$, and τ_p, respectively, under $Re = 200$, $F_c = 0.2$, and $L_c = 0.25$. In the steady state situation, the inlet cooling fluid directly impinges on the region close to the upper left corner which results in the maximum magnitude of the local Nusselt number logically occurring at the stated region. However, the cooling channel could be regarded as a confined channel and the Reynolds number is small which leads the rebound motion of the cooling fluid accompanying with the impingement mentioned above to be very slight. As a result, the distribution of the local Nusselt number monotonously decreases from the left to right region. Oppositely, in the reciprocating situation, the motions of the cooling fluid are affected apparently by the moving cooling channel, the rebound phenomenon accompanying with the impingement of the cooling fluid could be observed in the variations of streamlines shown in Fig. 3. Therefore, the second even third summits of the distributions of the local Nusselt number are found out on certain regions apart from the region of the maximum local Nusselt number at the $\tau_p/4$, $2\tau_p/4$, $3\tau_p/4$, and τ_p cycles, respectively.

In Fig. 5, as the frequency F_c decrease to 0.1, the motions of the cooling fluid affected by the cooling channel become weak which causes the rebound phenomenon in the cooling channel induced by the impingement of the cooling fluid to be slightly. Accordingly, the second and third summits of the distributions of the local Nusselt number are not remarkable as the above figure, and the distributions of the local Nusselt number of the reciprocating situation are similar to that of the stationary state.

In Fig. 6, as the frequency F_c increases to 0.4. Doubtless, the motions of the cooling fluid affected by the cooling channel are more drastic than these of the above cases. The remarkable magnitudes and variations of the distributions of the local Nusselt number are then obtained.

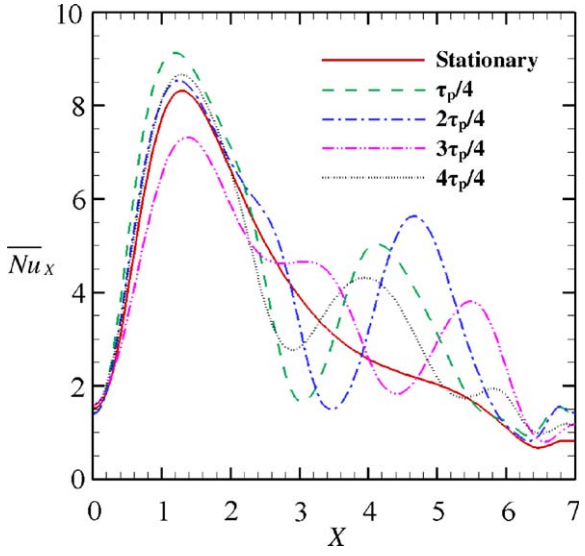

Fig. 4. The distributions of local Nusselt number on the top surface of the horizontal channel for case 2, $Re = 200$, $F_c = 0.2$, $L_c = 0.25$.

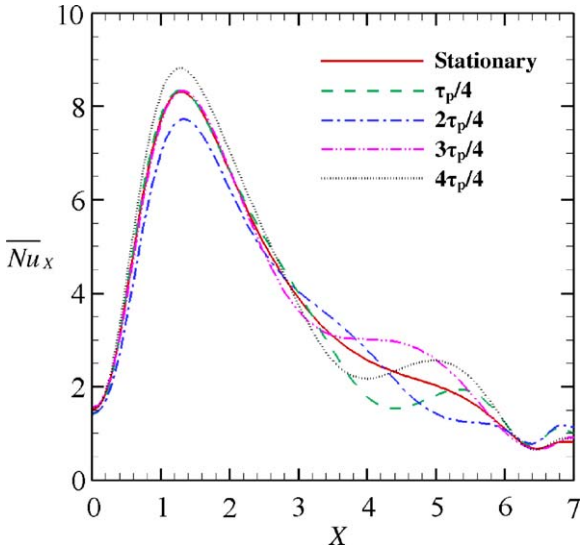

Fig. 5. The distributions of local Nusselt number on the top surface of the horizontal channel for case 1, $Re = 200$, $F_c = 0.1$, $L_c = 0.25$.

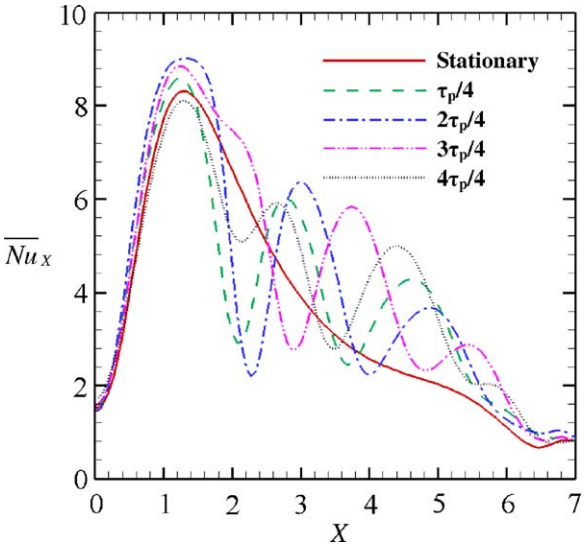

Fig. 6. The distributions of local Nusselt number on the top surface of the horizontal channel for case 3, $Re = 200$, $F_c = 0.4$, $L_c = 0.25$.

Fig. 7(a) indicates the variation of dimensionless mass flow rate $\dot{M}_{exit}$ at the exit of the cooling channel in a cycle time. As the cooling channel is at stationary state, the dimensionless mass flow rate $\dot{M}_{inlet}$ is constant and equal to 1 at the inlet of the cooling channel. Due to the conservation of mass, the mass flow rate at the exit of the cooling channel should be constant and equal to 1. However, the reciprocating motion of the cooling channel results in the volume of the cooling channel containing the cooling fluid being changed.

The mass flow rate at the exit of the cooling channel $\dot{M}_{exit}$ could be calculated by the following equation:

$$\dot{M}_{exit} = \dot{M}_{inlet} - 4\pi F_c L_c \sin(2\pi F_c \tau) \quad (23)$$

where

$$\dot{M}_{inlet} = \sum V_{n,inlet} \Delta W = V_0 W \quad (24)$$

$$\dot{M}_{exit} = \sum V_{n,exit} \Delta W \quad (25)$$

in which $V_{n,exit}$ is the local velocity at the exit on the X-axis, ΔW is the unit width of the exit.

The term of $4\pi F_c L_c \sin(2\pi F_c \tau)$ could be regarded as the variation of the volume of the cooling channel. In the former half periodical cycle ($\tau = 0 \sim \frac{\tau_p}{2}$), the volume of the cooling channel is enlarged. As a result, the cooling fluid flowing into the cooling channel is used to supplement the enlargement volume of the cooling channel which directly leads the mass flow rate at the exit of the cooling channel to be decreased. As the magnitude of $4\pi F_c L_c \sin(2\pi F_c \tau)$ is larger than that of $\dot{M}_{inlet}$, the value of $\dot{M}_{exit}$ becomes negative which means some cooling fluids are sucked from the surroundings and the mass flow rate distributed on the exit section could be shown in Fig. 7(b). Oppositely, in the later half periodical cycle ($\tau = \frac{\tau_p}{2} \sim \tau_p$), the velocity of the cooling channel is downward, and volume of the cooling channel is relatively contracted. Naturally, the quantity of the cooling channel is extraordinarily exhausted from the exit of the cooling channel which makes the mass flow rate to be larger than that of the stationary state.

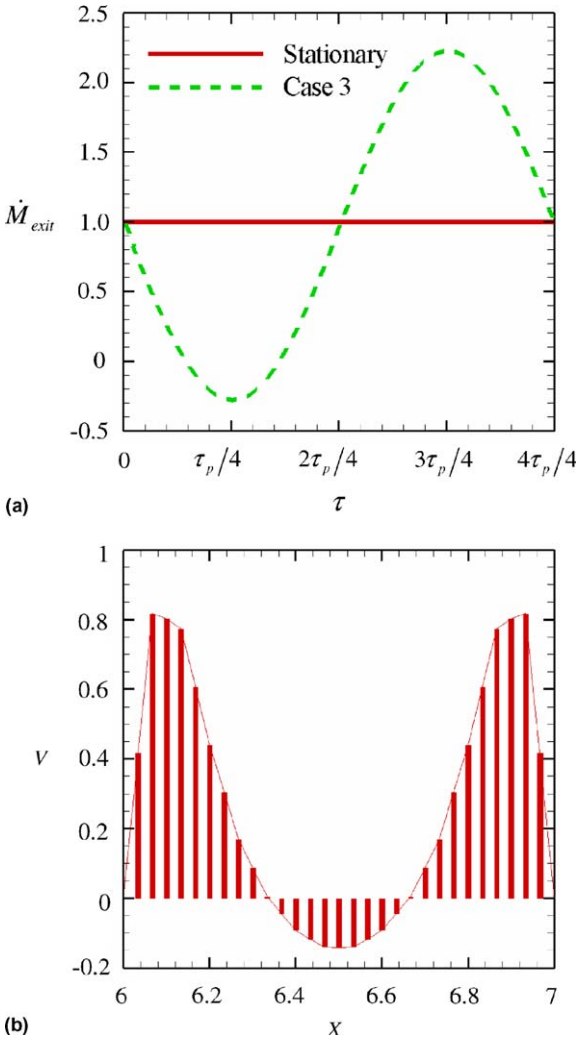

Fig. 7. (a) The variation of dimensionless mass flow rate $\dot{M}_{exit}$ at the exit of the cooling channel in a cycle time of case 3. (b) The vertical velocity profile at the outlet end of the channel at time $\tau_p/4$ of case 3.

Shown in Fig. 8, there are the distributions of the average Nusselt number $\overline{Nu}_X$ in three periodical cycles for $F_c = 0.1$, 0.2, and 0.4 under $Re = 200$, $L_c = 0.2$ situation, respectively. According to the relative velocity concept, the maximum magnitude of the average Nusselt number should be obtained while the moving directions of the cooling fluid and cooling channel are opposite. However, in the reciprocating situation due to the interaction of the cooling fluid and cooling channel the variations of the thermal boundary layer and velocity boundary layer are no longer synchronous which result in the maximum magnitude of the average Nusselt number occurring at different times in a periodical cycle. Besides, the variations of the magnitude of the maximum average Nusselt number and the distribution of average Nusselt number with time are seriously affected by the variation of frequency, and those

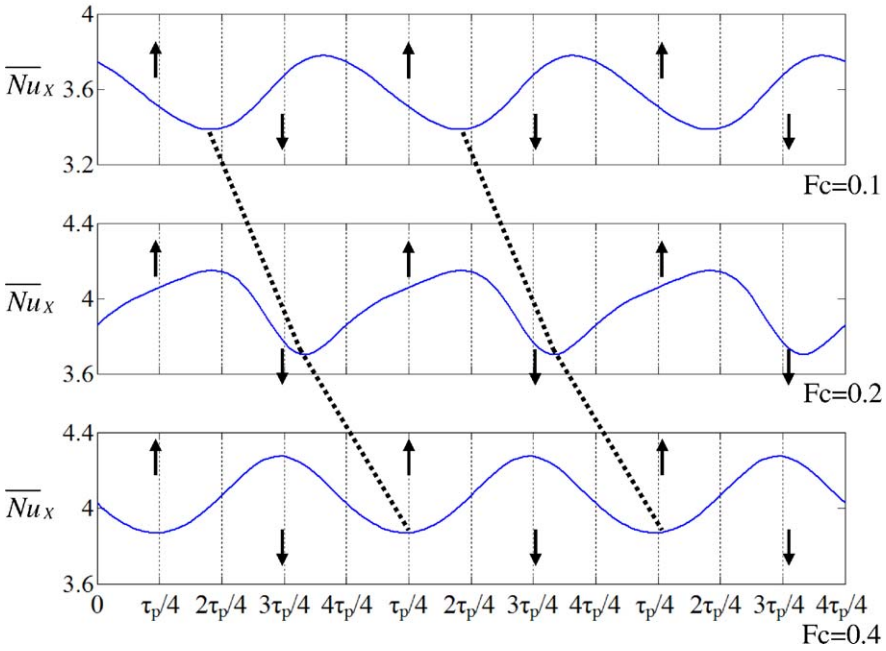

Fig. 8. The distributions of the average Nusselt number $\overline{Nu}_X$ in three periodical cycles for $F_c = 0.1$, 0.2, 0.4 under $Re = 200$ and $L_c = 0.25$ situation.

phenomena had been observed by Nishimura et al. [8]. Generally, the larger the frequency is, the larger the average Nusselt number is obtained.

Fig. 9 shows the distributions of the average Nusselt number $\overline{Nu}_X$ in three periodical cycle for $L_c = 0.25$, 0.5, and 1 under $Re = 200$, $F_c = 0.1$ situation, respectively. Since the frequency and Reynolds number are the same, the distributions of the average Nusselt number verse time are similar. According to the parameter combinations indicated in Table 1, the larger the L_c is, the larger V_m becomes. As a result, the maximum relative velocity between the cooling fluid and cooling channel occurs for the situation of the largest magnitude of the V_m which causes the maximum average Nusselt number distribution to be gained.

Fig. 10 shows the distributions of the average Nusselt number $\overline{Nu}_X$ in three periodical cycle for $Re = 200$, 500, and 750 under $L_c = 0.25$, $F_c = 0.1$ situation, respectively.

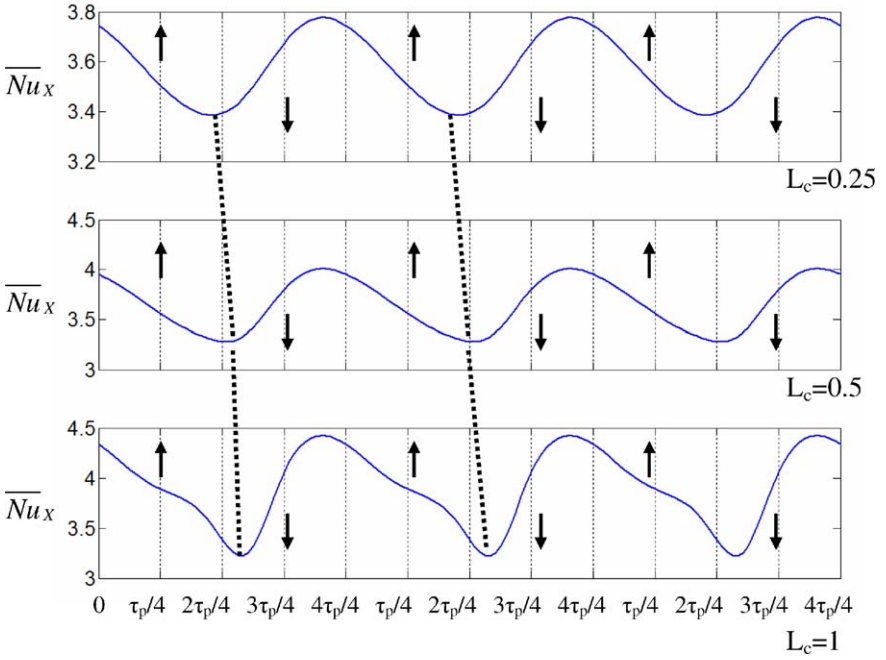

Fig. 9. The distributions of the average Nusselt number $\overline{Nu}_X$ in three periodical cycles for $L_c = 0.25$, 0.5 and 1 under $Re = 200$ and $F_c = 0.1$ situation.

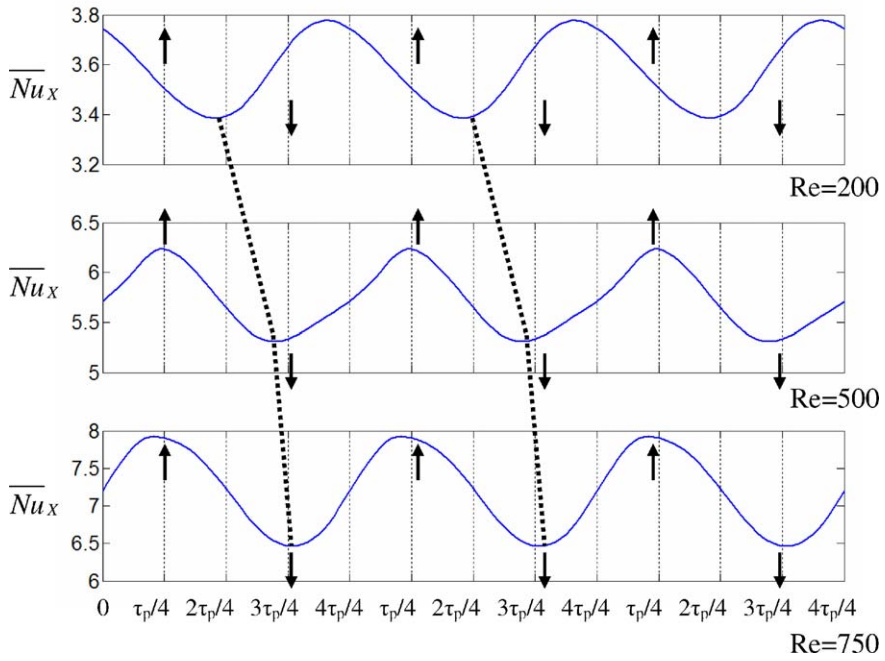

Fig. 10. The distributions of the average Nusselt number $\overline{Nu}_X$ in three periodical cycle for $Re = 200$, 500, and 750 under $L_c = 0.25$ and $F_c = 0.1$ situation.

The magnitude of V_m could be expressed in terms of $2\pi F_c L_c$, the values of V_m in the different Reynolds number cases are equal. Therefore, the Reynolds number directly dominates the magnitude of the average Nusselt number. Naturally, the larger the Reynolds number is, the larger the distribution of the average Nusselt number becomes. The distribution of the average Nusselt number verse time for $Re = 200$ situation has slight deviation from those of $Re = 500$ and 700 situations. The reason is suggested that the smaller Reynolds number situation causes the relative velocity effect to be not remarkable as the larger Reynolds number situations.

Fig. 11 indicates the cases of the distributions of the time-average Nusselt numbers verse time studied in this work. Generally, the larger the Reynolds number, frequency and amplitude are, the larger the time-average Nusselt number could be obtained. The maximum enhancement shown in Table 1 is about four times of the stationary case.

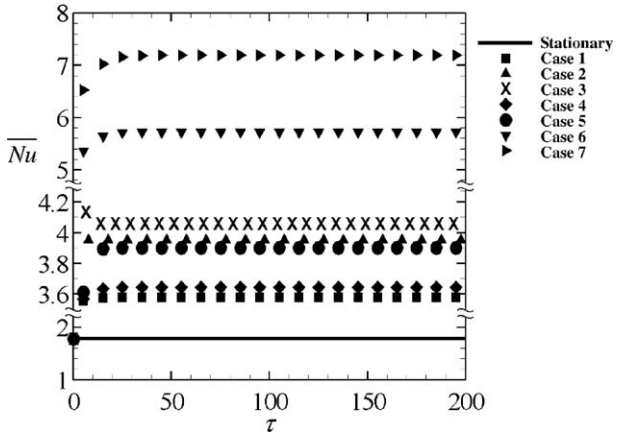

Fig. 11. All cases of the distributions of the time-average Nusselt numbers verse time studied in this work.

5. Conclusions

Heat transfer phenomena of the reciprocating piston cooled by the fluid are investigated numerically. The parameters of frequency, amplitude and Reynolds number are considered and the useful results are obtained and examined in detail. Some conclusions could be summarized as follows:

(1) The heat transfer mechanisms affected by the frequency are more remarkable than those affected by the amplitude and Reynolds number.
(2) The enlargement and contract of the volume of the cooling channel are accompanying with the upward and downward velocities of the cooling channel which cause the mass flow rate of the cooling fluid on the exit section to be varied periodically.
(3) Generally, the larger the frequency, amplitude and Reynolds number are, the apparent enhancements of the heat transfer rate are obtained.

Acknowledgement

The support of this study by the National Science Council of Taiwan, ROC, under contract NSC93-2212-E-009-010 is gratefully acknowledged.

References

[1] S.W. Chang, L.M. Su, Heat transfer in a reciprocating duct fitted with transverse ribs, Exp. Heat Transfer 12 (1999) 95–115.

[2] P.P. Grassmann, M. Tuma, Applications of the electrolytic method-II. Mass transfer within a tube for steady, oscillating and pulsating flows, Int. J. Heat Mass Transfer 22 (1979) 799–804.

[3] A.T. Patera, B.B. Mikic, Exploiting hydrodynamic instabilities resonant heat transfer enhancement, Int. J. Heat Mass Transfer 29 (8) (1986) 1127–1138.

[4] S.Y. Kim, B.H. Kang, A.E. Hyun, Heat transfer in the thermally developing region of a pulsating channel flow, Int. J. Heat Mass Transfer 36 (17) (1993) 1257–1266.

[5] T. Nishimura, N. Kojima, Mass transfer enhancement in a symmetric sinusoidal wavy-walled channel for pulsatile flow, Int. J. Heat Mass Transfer 38 (9) (1995) 1719–1731.

[6] T. Nishimura, A. Taurmoto, Y. Kawamura, Flow and mass transfer characteristics in wavy channels for oscillatory flow, Int. J. Heat Mass Transfer 38 (1987) 1007–1015.

[7] T. Nishimura, S. Arakawa, D. Murakami, Y. Kawamura, Oscillatory flow in a symmetric sinusoidal wavy-walled channel at intermediate strouhal numbers, Chem. Eng. Sci. 46 (1991) 757–771.

[8] T. Nishimura, S. Arakawa, D. Murakami, Y. Kawamura, Oscillatory viscous flow in symmetric sinusoidal wavy-walled channels, Chem. Eng. Sci. 44 (1989) 2137–2148.

[9] C.P. Chiu, Y.S. Kuo, Study of turbulent heat transfer in reciprocating engine using as algebraic grid generation technique, Numer. Heat Transfer, Part A 27 (1995) 255–271.

[10] S.W. Chang, L.M. Su, Influence of reciprocating motion on heat transfer inside a ribbed duct with application to piston cooling in marine diesel engines, J. Ship Res. 41 (4) (1997) 332–339.

[11] C.H. Cheng, C.K. Hung, Numerical predictions of flow thermal fields in a reciprocating piston-cylinder assembly, Numer. Heat Transfer, Part A 38 (2000) 397–421.

[12] C. Sert, A. Beskok, Oscillatory flow forced convection in micro heat spreaders, Numer. Heat Transfer, Part A 42 (2002) 685–705.

[13] A.R.A. Khaled, K. Vafai, Heat transfer and hydromagnetic control of flow exit conditions inside oscillatory squeezed thin films, Numer. Heat Transfer, Part A 43 (2003) 239–258.

[14] S.W. Chang, L.M. Su, W.D. Morris, T.M. Liou, Heat transfer in a smooth-walled reciprocating anti-gravity open thermosyphon, Int. J. Heat Mass Transfer 42 (2003) 1089–1103.

[15] J.N. Reddy, D.K. Gartling, in: The Finite Element Method in Heat Transfer and Fluid Dynamics, CRC Press, Ann Arbor, 1994, pp. 47–51.

[16] W.S. Fu, T.M. Kau, W.J. Shieh, Transient laminar natural convection in an enclosure from steady state to stationary state, Numer. Heat Transfer, Part A 18 (1990) 189–212.